Journal Homepage: http://ijcpe.uobaghdad.edu.iq
Iraqi Journal of Chemical and Petroleum Engineering
Vol. 26 No. 3 (September 2025) 19 – 28
EISSN: 2618-0707, PISSN: 1997-4884

Photocatalytic degradation of methylene blue by robust visible-light-driven polyvinylidene fluoride membranes incorporating Ag_2O@CRA photocatalyst: Kinetics analysis and cost assessment

Abdelmoneim S. Adday [a], Sama M. Al-Jubouri [a, *], Sirhan Al-Batty [b]

a Department of Chemical Engineering, College of Engineering, University of Baghdad, Baghdad, Iraq
b Department of Chemical Engineering, Jubail Industrial College, Jubail, Saudi Arabia

Abstract

The kinetic study of the visible-light-driven photocatalytic degradation of methylene blue (MB) dye by the Ag_2O@CRA heterojunction photocatalyst and robust polyvinylidene fluoride membranes incorporating Ag_2O@CRA heterojunction photocatalyst (PVDF/Ag_2O@CRA) was investigated. This study involves a comparison of the outcomes of the kinetic study performed based on the experimental data of the oxidative photocatalytic degradation of the MB dye. The zero-order, pseudo-first-order, and modified Freundlich kinetic models were applied to accomplish this study. The results showed that the photocatalytic oxidation of the MB dye by the Ag_2O@CRA photocatalyst followed the pseudo-first-order kinetic model, and the apparent rate constant (k_1) value was 0.1231 min^{-1}. The photocatalytic oxidation of the MB dye by the modified PVDF membrane with 0.3 wt.% Ag_2O@CRA photocatalyst followed the pseudo-first-order kinetic model, and the apparent rate constant (k_1) value was 0.0196 min^{-1}. Also, the Langmuir-Hinshelwood model was used to model the MB photocatalytic degradation kinetics by the Ag_2O@CRA photocatalyst for 10-40 mg/L inlet MB concentrations. Likewise, the Langmuir-Hinshelwood model was used to model the kinetics of the MB photocatalytic degradation by the PVDF membrane with 0.3 wt.% Ag_2O@CRA photocatalyst for 5-20 mg/L inlet MB concentrations. It was found that the intrinsic photocatalysis reaction rate constant (kr) was 0.8286 mg/L.min for the Ag_2O@CRA heterojunction photocatalyst and 0.209 mg/L.min for the PVDF/Ag_2O@CRA photocatalytic membrane. Also, it was found that the equilibrium adsorption constant ($K_{ad.}$) was 0.3245 L/mg for the Ag_2O@CRA heterojunction photocatalyst and 0.218 L/mg for the PVDF/Ag_2O@CRA photocatalytic membrane. The manufacturing cost for the Ag_2O@CRA photocatalyst and PVDF/Ag_2O@CRA photocatalytic membrane was estimated to be \$2.45/10 g and \$78/m², respectively.

Keywords: Kinetics, oxidation; heterojunction photocatalyst; photocatalytic membrane; polyvinylidene fluoride; methylene blue.

Received on 31/03/2025, Received in Revised Form on 25/06/2025, Accepted on 26/06/2025, Published on 30/09/2025

https://doi.org/10.31699/IJCPE.2025.3.3

1- Introduction

The environment, water resources, and living beings are threatened by the risk of pollution resulting from unplanned urbanization, industrial activities, and overpopulation [1]. Agricultural prosperity and rapid industrialization make the water streams accessible to numerous pollutants such as bacteria, biological substances, heavy metals, microplastics, oil, viruses, and other harmful compounds [2, 3]. Wastewater polluted by organic dyes poses a factual challenge to the environment because it contains substantial quantities of stubborn coloured solutions infiltrated by industries [4]. The industrial wastewater pumped into the environment holds about 10%-15% of the dyes used in the processes that deal with dyes, and ultimately turns into waste material [5]. For long-term exposure, pollution by dyes can lead to diverse antagonistic effects on human beings, for example, allergic diseases, dermatitis, eye irritation, etc. [6].

Dyes are important for coloring items such as cosmetics, food, leather processing, paper, pharmaceutical products, printing, tannery, textile fibers, etc. [7, 8]. The significant problem of releasing dyes in the aquatic environment stems from their high toxicity, low biodegradability, and stability against heat and light [9]. Besides natural dyes, synthetic dyes are a wide range of colours synthesized from organic compounds and used in various applications [10]. Dyes can be one of the following main classes: (i) anionic dyes, which include acid, direct, and reactive dyes, having a negative charge mainly because of SO^{3-}group, (ii) cationic or basic dyes because of having a protonated amine group, and (c) nonionic dyes (disperse dyes) depending on their dissociation manner in the aqueous solutions. Azo dyes (cationic or anionic) produce one or even more azoic bonds ($N = N$) [11].

Methylene blue (MB) is a basic, cationic, photosensitive, and azo dye; its commercial form is

*Corresponding Author: Email: sama.al-jubouri@coeng.uobaghdad.edu.iq

exploited in various industrial, medical, and pharmaceutical products. MB dye is mostly consumed in the clothing and textile industries to dye cotton, linen, silk fabrics, and wool [12]. In contrast to the intake of MB in polluted water, it has medical uses and can be safely used when clinically prescribed. Therefore, it is used for treating Alzheimer, heparin neutralization, methemoglobinemia, malaria (a treatment dosage of 36-72 mg/kg over 3 days), and vasoplegia post-transplant operation. In addition, it is an oral intake to diagnose the areas of plaque microbial teeth [13].

Despite the beneficial uses of MB dye, releasing untreated MB dye-contained wastewater within the industrial effluents could result in several health hazards such as breathing problems, cyanosis, eye burns, intestine complications, nausea, mental disorder, severe sweating, skin irritation, tissue necrosis, vomiting, cardiovascular disorders including anemia, dizziness, fever, headache, and hypertension [14, 15]. Other consequences of the presence of dyes in the surface water bodies are repulsive color, increased water hardness and turbidity, and overfeeding (excessive and rapid growth of algae) due to disabling the photosynthesis process by impeding sunlight breakthrough to the water body [16]. Consequently, effectively removing MB dye from wastewater before industrial discharge to eliminate its negative effects becomes crucial.

Various biological, chemical, and physical technologies have been examined to purify the textile effluents polluted by organic dyes, such as adsorption, coagulation, filtration, ion-exchange, oxidation, sedimentation, etc. [17]. Some of these techniques showed drawbacks associated with biological and chemical stiffness of the dyes, unqualification for treating high concentrations, generation of secondary wastes which require further treatment, and treatment cost [18]. So far, recent studies have been keen to develop a renewed treatment method that guarantees the complete elimination of organic pollutants from the waste effluents, such as advanced oxidation processes (AOPs), which include catalytic wet air oxidation, Fenton process, electrochemical oxidation, ozone-based processes, and photo-oxidation processes [19]. AOPs involve the generation of hydroxyl radical (OH•) as a primary oxidant because it is a highly reactive and nonselective oxidant, which allows the decomposition of many organic compounds simultaneously [20]. Nevertheless, almost all AOPs have the drawbacks of hard catalyst separation at the end of the process, limited treated effluent size, and losses of the catalyst during the regeneration process [21].

Also, the application of membrane filtration techniques in the removal of some organic compounds has become widespread because of the simple operation and handling, low power consumption, and large treated effluent size [22, 23]. However, the major drawback of implementing the membrane filtration process is fouling, which minimizes the treated effluent size, raises the operation cost, reduces the membrane lifespan, and sometimes leads to deterioration of the quality of filtrate [23]. Accordingly, combining the advantages of photocatalytic degradation and filtration membrane technologies by constructing new multifunction membranes implanted with photoactive catalysts has emerged as a new effective route in wastewater treatment technologies, which ensures complete elimination of harmful organics.

This work involves studying the kinetic behaviour of the photocatalytic degradation process of the MB dye conducted via the Ag_2O@CRA heterojunctions photocatalyst and the PVDF/Ag_2O@CRA photocatalytic membrane. Three kinetic models, including the zero-order, pseudo-first order, and modified Freundlich kinetic models, were used to assess the photocatalytic degradation performance to understand the kinetic behaviour of the photocatalytic degradation process. Also, for more elucidation of the kinetic behaviour of photocatalysis by the developed photocatalyst and photocatalytic membrane, the first-order kinetic equation of the Langmuir-Hinshelwood was applied for various initial MB concentrations to determine the actual rate constant of the photocatalysis reaction. What is more, the cost of the synthesized Ag_2O@CRA photocatalyst and the PVDF/Ag_2O@CRA photocatalytic membrane was investigated.

2- The photocatalysis reaction kinetics

Reaction kinetics is one of the fundamental aspects of reactor engineering because kinetics provides a quantitative or qualitative evaluation of the rate of reactions, and insight into the variables that the reaction rate depends on, such as light intensity, targeted pollutant concentration, pH, and temperature [24–26]. Comprehension of the reaction kinetics is crucial for managing the reaction and achieving the purposive yield. Several kinetic models have been developed to determine the rate constants required for the reactor design, even though some assumptions made to determine the reaction kinetics may not fit the real reactors, since ideal mass transfer and mixing cannot be attained in non-perfect situations [27, 28]. It is worth mentioning that the close matching of the kinetic parameters to the data does not necessarily mean the solution exactly seizes the actual kinetic sequence [29]. Therefore, various kinetic models must be developed, examined, and compared with each other to trust the kinetic model.

The mathematical form of the kinetic models, which were applied to the data of photocatalytic degradation of MB dye by both Ag_2O@CRA photocatalyst and PVDF/Ag_2O@CRA membrane, is presented in Eqs. 1 - 3, respectively. The zero-order model is given by Eq. 1 [30, 31].

$$C_{MBo} - C_{MBt} = k_o.t \quad (1)$$

The pseudo-first-order model is given by Eq. 2 [25].

$$ln(C_{MBo}/C_{MBt}) = k_1.t \quad (2)$$

The modified Freundlich model is given by Eq. 3 [32].

$$C_{MBt} = k_{Fr}.C_{MBo}.t^{1/m} \quad (3)$$

The linearized form of the modified Freundlich model can be given by Eq. 4.

$$\ln(C_{MBt}) = \ln(k_{Fr}.C_{MBo}) + (1/m)\ln(t) \quad (4)$$

Where C_{MBo} and C_{MBt} are the MB dye concentration (mg/L) at zero and t is the time of irradiation (min). k_o (mg/L.min), k_1 (min^{-1}), and k_{Fr} (min$^{-1/m}$) are the apparent constants of the zero-order, pseudo-first-order, and modified Freundlich models, respectively. m is the modified Freundlich exponent [33].

3- Experimental work

The data used for studying the kinetics of the MB photocatalytic degradation by the Ag_2O@CRA heterojunction photocatalyst were obtained from the batch study presented in the previous work [34]. However, the kinetics of the MB photocatalytic degradation by the PVDF/Ag_2O@CRA photocatalytic membrane was conducted based on the data extracted after stopping the filtration role of the PVDF/Ag_2O@CRA membrane but allowing the continuity of the photocatalysis effect of the developed membrane. The developed PVDF membranes containing 0.1 wt.%, 0.3 wt.%, and 0.5 wt.% Ag_2O@CRA heterojunctions photocatalysts were determined to be PM1, PM3, and PM5, respectively. Moreover, the developed PVDF membrane by 0.3 wt.% CRA was determined to be PMS. The photocatalysis performance of the PVDF/Ag_2O@CRA photocatalytic membranes was studied in a batch cylindrical Pyrex flask irradiated with visible light 50 Watts, at a 10 cm distance from the liquid surface, as shown in Fig. 1. An 8.4 cm² piece of the photocatalytic membrane was submerged in 100 mL of 5 mg/L MB dye solution at room temperature. The visible light was activated after achieving adsorption equilibrium, and the photocatalytic degradation process proceeded for 90 min. The concentration of the MB dye was measured every 10 min using a UV-vis spectrophotometer UV-9200, at a wavelength of 664 nm.

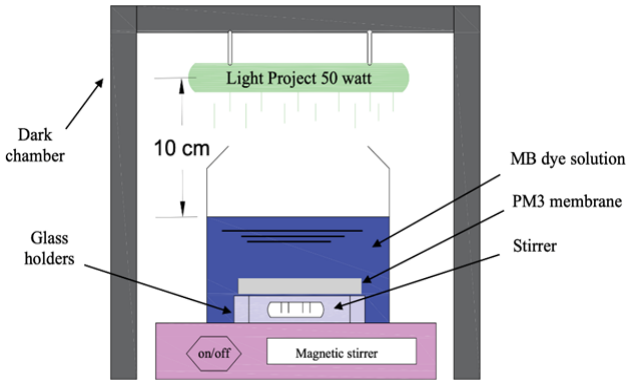

Fig. 1. A batch reactor for studying the kinetics of the photocatalytic activity of the PM3 membrane

Furthermore, the kinetics of the MB photocatalytic degradation for the PM3 membranes using the Langmuir-Hinshelwood kinetic equation was studied for the inlet MB concentrations of 5-20 mg/L at room temperature and under visible light.

4- Results and discussion

4.1. The photocatalysis reaction kinetics

The plots of fitting the kinetic models for the photocatalytic degradation of the MB by the CRA and Ag_2O@CRA photocatalyst are shown in Fig. 2, and the determined model parameters are presented in Table 1. The obtained results imply that all three models fitted the dye removal data with reasonable correlation coefficients (R^2) in the range of 0.812 - 0.997. However, a fair comparison made based on R^2 values indicated that the pseudo-first-order model has a comparatively better fit with the photocatalytic oxidative data of MB than the other models. Table 1 shows that the values of the rate constant for the MB photocatalytic degradation by the Ag_2O@CRA photocatalyst were higher than those of the rate constant for the photocatalytic degradation by the CRA, which explains the poor degradation of MB dye by the CRA because of its relatively large band gap (4.2 eV) [34]. Since rapid photocatalytic degradation can be obtained at a higher rate constant, as stated and agreed with Kusworo et al., [31].

Fig. 3 shows the plots that fit the kinetic models for the photocatalytic degradation of MB dye by the developed PVDF/Ag_2O@CRA photocatalytic membranes. The fitting parameters of the studied models are presented in Table 1. For all developed PVDF/Ag_2O@CRA photocatalytic membranes, Table 1 shows that R^2 values were the highest for the pseudo-first-order model (0.915 - 0.996) compared with the other studied models, which can be attributed to the low concentrations of the pollutant. This means all the examined membranes in the photocatalytic degradation of MB dye followed pseudo-first-order kinetics. It was observed that the assessed value of the rate constant for the photocatalytic degradation by the PM3 membrane was the highest compared with other developed PVDF/Ag_2O@CRA photocatalytic membranes. The PM3 membrane exhibited the highest rate constant with a value of 0.0196 min^{-1}, confirming it has a powerful photocatalytic ability that led to a faster photocatalytic degradation performance of MB dye. According to the assessed values of the rate constants, the examined photocatalytic membranes showed the following order: PM3 > PM1 > PM5. These results can be attributed to the embedding of the 18% PVDF membrane by more than 0.3 wt.% of the Ag_2O@CRA photocatalysts reduced the photon penetration through the photocatalyst membrane reactor and thus reduced the photocatalytic degradation of the MB dye. Furthermore, a surplus photocatalyst content in the photocatalytic membrane may result in agglomeration of the photocatalyst particles, which minimizes the surface area of exposure of the photocatalysis sites to the light photons to commence the photodegradation process. Therefore, the quantity of the Ag_2O@CRA heterojunction

photocatalyst must be optimized to guarantee the absorption of sufficient light photons for effective photomineralization. Therefore, the PM3 membrane consisting of 0.3 wt.% Ag_2O@CRA heterojunctions photocatalyst was the best among other membranes. Also, the low photocatalyst content (less than 0.3%) was insufficient relative to the pollutant concentration, resulting in limited catalysis sites for photocatalytic reactions. This imbalance reduces the degradation rate and extends the time required for effective pollutant removal. Therefore, the results of the kinetic study agreed with the results of the membranes' performance presented in the previous work [35].

The PMS membrane exhibited the lowest rate constant (0.0053 min^{-1}) because it contains CRA, which has low photocatalytic properties as presented in previous work [35]. It is worth noting that the rate constant of the PM3 membrane (0.0196 min^{-1}) was comparatively low when compared with that of the Ag_2O@CRA photocatalyst (0.1231 min^{-1}) because of its low content of this photocatalyst (0.3 wt.%). On the other hand, the PM3 membrane exhibited a comparatively higher rate constant than others calculated in previous studies involving PVDF-based photocatalytic membranes, as shown in Table 2.

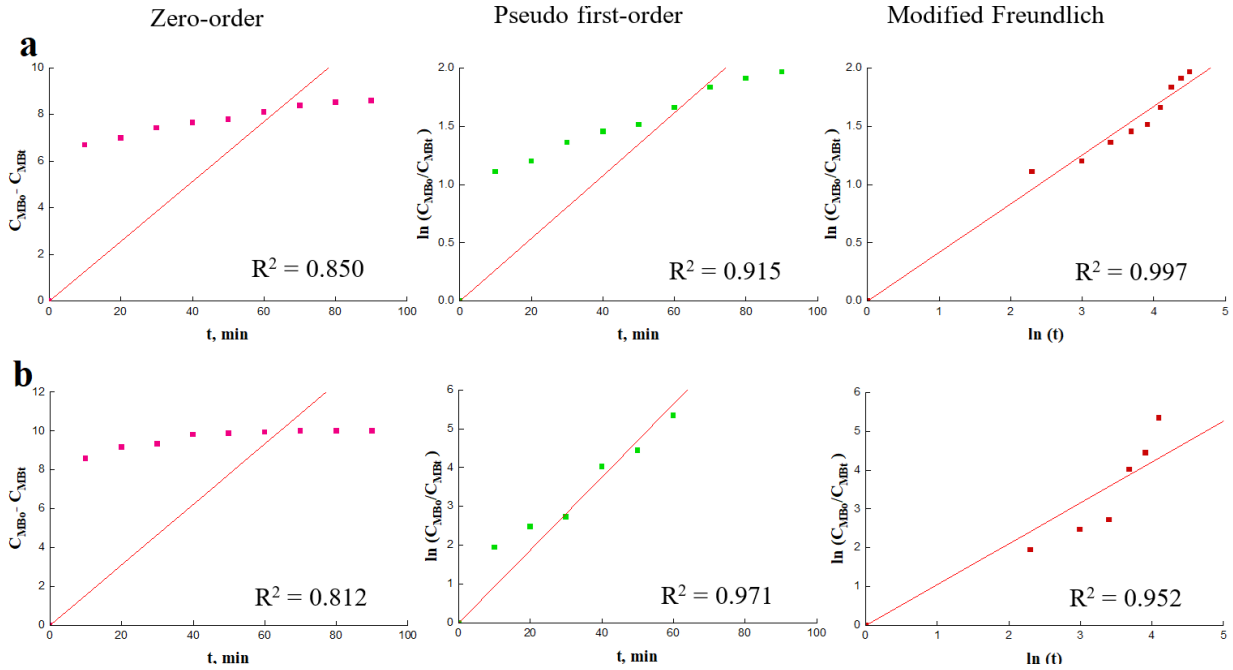

Fig. 2. The plots of fitting the kinetic models for: (a) CRA, and (b) Ag_2O@CRA photocatalyst

Table 1. The determined parameters of the kinetic models studying the photocatalytic degradation of the MB dye

Kinetics model	Model parameters and R^2	CRA	Ag_2O@CRA photocatalyst	PMS membrane	PM1 membrane	PM3 membrane	PM5 membrane
Zero order	k_o (mg/L.min)	0.128	0.1567	0.0222	0.0408	0.054	0.0303
	R^2	0.850	0.812	0.991	0.933	0.962	0.962
Pseudo-first-order	k_1 (min^{-1})	0.027	0.1231	0.0053	0.012	0.0196	0.0078
	R^2	0.915	0.971	0.996	0.991	0.995	0.979
Modified Freundlich	k_{Fr} ($min^{-1/m}$)	0.417	1.0809	0.0783	0.1727	0.2807	0.1147
	R^2	0.997	0.952	0.930	0.973	0.929	0.963

Moreover, the Langmuir-Hinshelwood kinetic model (Eq. 5) describes the relationship between the initial pollutant concentration and the photocatalytic degradation rate [40].

$$r_{MB} = -dC_{MB}/dt = (k_r K_{ad}/(1 + K_{ad} C_{MB0}))C_{MB}^n \quad (5)$$

Where k_r represents the actual photocatalysis reaction rate constant (mg/L.min) and $K_{ad.}$ represents the Langmuir-Hinshelwood constant of adsorption (L/mg). To solve Eq. 5, Ćelić et al. [41] assumed the first-order reaction kinetics. However, Chakachaka et al. [25] simplified Eq. 5 to Eq. 6 by assuming a low initial concentration of the targeted pollutant; consequently, the rate of reaction will be dependent on reaction time rather than the concentration of the pollutant.

$$r_{MB} = k_r . K_{ad.} C_{MB} \quad (6)$$

Herein, the above results demonstrated that the reaction kinetics of the MB photocatalytic degradation by the PM3 photocatalytic membrane followed the pseudo-first-order model. Therefore, the n value in Eq. 5 was set to 1, and the rate of reaction is as shown in Eq. 7, which was also reported by Utomo et al. [39] and Azarniya et al. [42]:

$$r_{MB} = k_1 . C_{MB} \quad (7)$$

Therefore:

$$k_1 = k_r K_{ad.}/(1 + K_{ad.} C_{MB0}) \quad (8)$$

$$1/k_1 = 1/k_r K_{ad.} + (1/k_r) C_{MB0} \quad (9)$$

The values of k_r and $K_{ad.}$ in Eq. 9 can be found by the linear plot of $1/k_1$ vers C_{MB0}.

Table 3 shows that the apparent rate constant decreased with increasing initial MB dye concentration and thus reduced the photocatalytic effectiveness. This can be attributed to the excessive pollutant concentrations, which slow the photocatalytic degradation rate because they can vary the solution's impenetrability, and consequently, pollutants absorb light instead of the photocatalyst. Chakachaka et al., [25] reported that the photocatalytic degradation reaction is sped up by raising the initial pollutant concentration within a limited range because high concentration increases the chances of effective collisions between oxidative radical species and target pollutants. Also, this table presents the values of k_r were 0.8286 and 0.2090 mg/L.min for the Ag_2O@CRA heterojunction photocatalyst and the PVDF/Ag_2O@CRA photocatalytic membranes, respectively. At the same time, the values of $K_{ad.}$ were 0.3245 and 0.2180 L/mg for the Ag_2O@CRA heterojunction photocatalyst and the PVDF/Ag_2O@CRA photocatalytic membranes, respectively, which indicate the predominant effect of the photocatalytic degradation reaction.

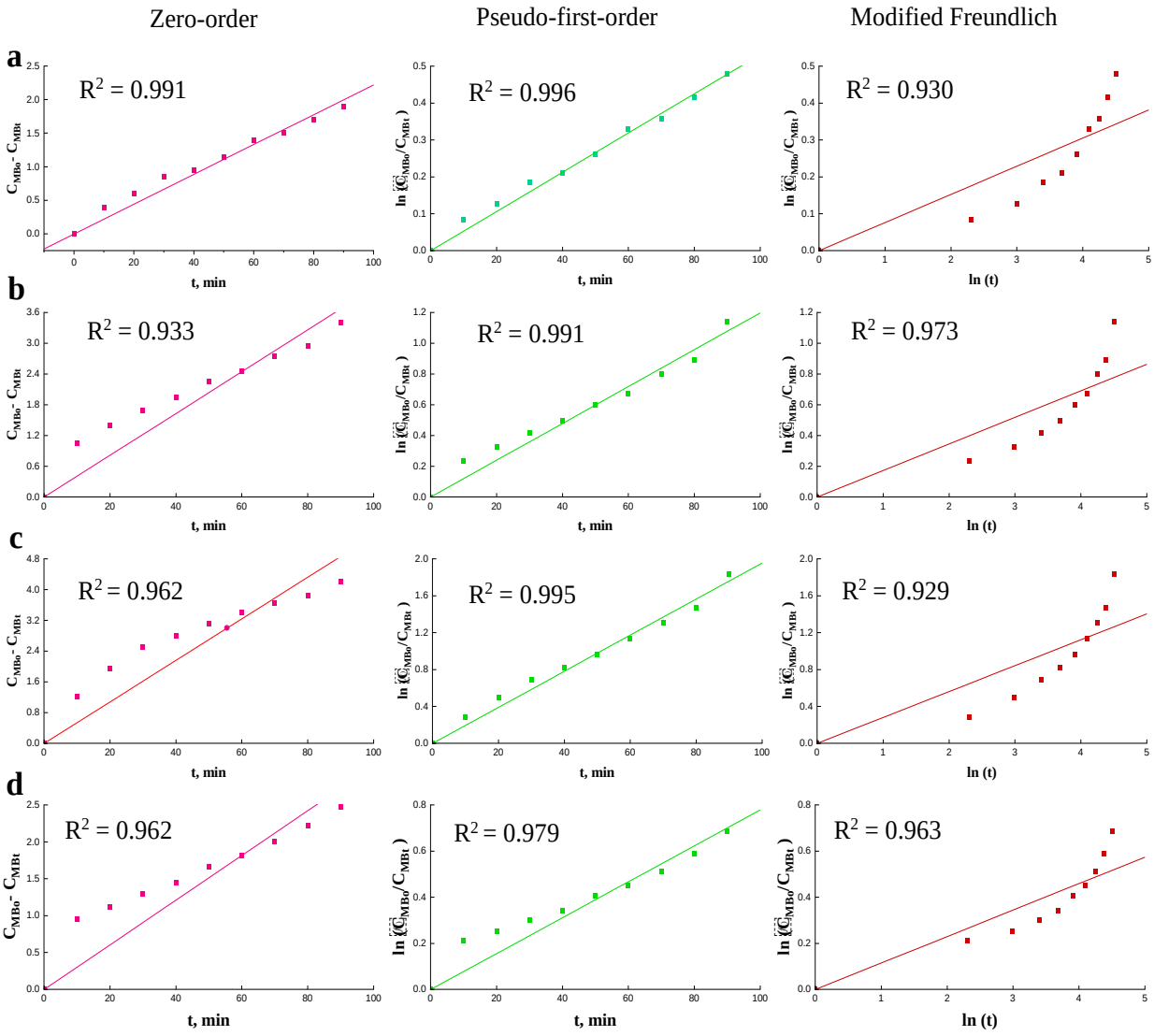

Fig. 3. The plots of fitting the kinetic models for: (a) PMS, (b) PM1, (c) PM3, and (d) PM5 membranes

Table 2. Comparison based on the apparent rate constant of the pseudo-first-order model

Photocatalytic membrane	Pollutant	k_1 (min^{-1})	Reference
(16 %) PVDF/(1 %) TiO_2	Congo red	0.0061	[36]
(16 %) PVDF/(2 %) $NiFe_2O_4$/(2 %)GO	Industrial dye wastewate	0.0088	[32]
PVDF/(0.5 g)NCQDs-BiOBr-TiO_2	Tetracycline	0.01342	[37]
(17 %)PVDF/(2 %) MoS_2@WO_3	Natural rubber wastewater	0.00293	[38]
(18 %)PVDF/(4 %) CeO_2@GO-COOH	Ciprofloxacin Sulfanilamide	0.0121 0.0122	[39]
(18 %)PVDF/(0.3 %) Ag_2O@CRA	Methylene blue	0.0196	Current work

Table 3. The apparent rate constant and the Langmuir-Hinshelwood model constants of the MB photocatalytic degradation by the Ag_2O@CRA heterojunction photocatalyst and the PM3 photocatalytic membrane

Initial MB dye concentration (mg/L)	Ag_2O@CRA heterojunction photocatalyst		Initial MB dye concentration (mg/L)	The PM3 photocatalytic membrane	
	k_1 (min^{-1})	R^2		k_1 (min^{-1})	R^2
10	0.1231	0.970	5	0.0196	0.995
20	0.0948	0.980	10	0.0150	0.987
30	0.0474	0.957	15	0.0120	0.993
40	0.0325	0.953	20	0.0080	0.991
	k_r = 0.8286 mg/L.min			k_r = 0.2090 mg/L.min	
	$K_{ad.}$ = 0.3245 L/mg			$K_{ad.}$ = 0.2180 L/mg	

4.2. Estimation of the manufacturing cost of the Ag_2O@CRA photocatalyst and PM3 membrane

The overall manufacturing cost of the Ag_2O@CRA photocatalyst and PM3 membrane was calculated using Eq.10 and Eq. 11, considering that the official electricity rate for government institutions in Iraq is 120 IQD/kWh, which is 0.09091 $/kWh [43]. The prices of the materials utilized in the membrane production were established based on local store sales.

$$C_t = C_m + C_p \quad (10)$$

$$C_p = P_i * C_{op} \quad (11)$$

Where C_t represents the overall manufacturing cost ($), C_m denotes the total cost of materials ($), C_p signifies the total cost of the used electrical power ($), P_i indicates the power of instruments utilized in membrane manufacture (kWh), and C_{op} refers to the official price of power ($/kWh). The overall expense of the utilized electrical energy encompassed the power consumed during the preparation of the polymeric solution and photocatalyst (including sonication, drying, furnace operation, and stirring). Also, the membrane fabrication process (casting) was based on the duration allocated to each process, as shown in Table 4 to Table 7. The calculated cost of manufacturing the Ag_2O@CRA photocatalyst was $2.45/10 g. While, the cost of manufacturing the PM3 membrane was $78/$m^2$. The cost of the PM3 membrane was very close to the price of the modified PVDF by SnO_2 nanoparticles prepared in a work published by Saleem and Al-Jubouri [1].

In terms of initial cost per unit, the photocatalyst ($2.45 /10 g) is markedly less expensive than the PM3 membrane ($78 /m²); however, for applications demanding extended operational lifespan and minimal maintenance expenditure over multiple years, the PM3 membrane may prove superior despite its higher capital cost. Consequently, the most economically viable choice depends on three critical parameters: the consumption rate (quantity of catalyst or membrane area required), the service life (number of operational cycles before maintenance or replacement), and the associated operational and maintenance costs (such as catalyst separation or membrane cleaning and energy consumption).

Table 4. Cost assessment of the Ag_2O@CRA photocatalyst

User device	Time	Power			
	h	W	W	Wh	$/kWh
Furnace	6	3000-6000	4500	27000	27
Total cost of the Ag_2O@CRA photocatalyst $/10 g					2.45

Table 5. Cost assessment of the materials used for PM3 membrane preparation

Materials	Used quantities		Price	Price of the used quantity
	wt.%	g	$/g	$
PVDF	18	3.6	1.515	5.454
DMF	81.7	16.34	0.074	1.209
Ag_2O@CRA	0.3	0.06	0.245	0.015
Total price				$6.68

Table 6. Cost assessment of the power used in the PM3 membrane preparation

Device	Operating time (h)	Device power (W)	Consumed electrical power (kwh)	Cost of consumed electrical power ($)
Ultrasonic	2	500	1	0.091
Dryer	5	1000	5	0.455
Magnetic Stirrer	37	450	16.65	1.514
Casting Machine	0.5	370	0.185	0.017

Table 7. Total cost of the prepared PM3 membrane

Cost of the used materials	$6.68
Cost of the used power	$2.08
Total cost of the PM3 membrane	$8.75
Total cost of the PM3 membrane	$78/$m^2$

5- Conclusion

In conclusion, the kinetics of the photocatalytic degradation reaction of the MB dye by the Ag_2O@CRA heterojunction photocatalyst and the flat sheet PVDF/Ag_2O@CRA photocatalytic membranes driven by visible-light irradiation have been investigated and elucidated in the current study. The zero-order, pseudo-first-order, and modified Freundlich kinetic models were fitted to the experimental data. The pseudo-first-order kinetics model matched the results of the MB dye photocatalytic degradation reaction by the Ag_2O@CRA heterojunction photocatalyst and the PVDF/Ag_2O@CRA photocatalytic membranes with high R^2 values. The apparent rate constants of the first-order model of the Ag_2O@CRA heterojunction photocatalyst and the PVDF/Ag_2O@CRA photocatalytic membranes were the highest because they have improved band gaps.

Moreover, the MP3 membrane showed the highest apparent rate constant (0.0196 min^{-1}) and rapid photocatalytic degradation reaction rate. Studying the influence of the initial dye concentration showed that increased concentration decelerated the photocatalytic degradation rate. Also, applying the Langmuir-Hinshelwood model showed that the intrinsic photocatalysis reaction rate constants were 0.8286 and 0.2090 mg/L.min for the Ag_2O@CRA heterojunction photocatalyst and the PVDF/Ag_2O@CRA photocatalytic membranes, respectively. Also, the equilibrium adsorption constants were 0.3245 and 0.2180 L/mg for the Ag_2O@CRA heterojunction photocatalyst and the PVDF/Ag_2O@CRA photocatalytic membranes, respectively. The estimated manufacturing costs of the Ag_2O@CRA photocatalyst and PVDF/Ag_2O@CRA photocatalytic membrane were \$2.45/10 g and \$78/m^2, respectively.

References

[1] A.G. Saleem, S.M. Al-Jubouri, S. Al-Batty, M. Wali Hakami, Determination of controlling fouling mechanism using the Hermia models and estimation of the manufacturing costs of the modified polyvinylidene fluoride-based ultrafiltration membranes, *Iraqi Journal of Chemical and Petroleum Engineering*, 26, 2025, 67–76, https://doi.org/10.31699/IJCPE.2025.1.7

[2] S.M. Al-Jubouri, S.I. Al-Batty, R. Ramsden, J. Tay, S.M. Holmes, Elucidation of the removal of trivalent and divalent heavy metal ions from aqueous solutions using hybrid-porous composite ion-exchangers by nonlinear regression, *Desalination and Water Treatment*, 236, 2021, 171–181, https://doi.org/10.5004/dwt.2021.27707

[3] S.M. Abbas, S.M. Al-Jubouri, High performance and antifouling zeolite@polyethersulfone/cellulose acetate asymmetric membrane for efficient separation of oily wastewater, *Journal of Environmental Chemical Engineering*, 12, 2024, 112775. https://doi.org/10.1016/j.jece.2024.112775

[4] A.B. Salman, S.N. Abdulqahar, Electrochemical oxidation of methyl blue dye using stainless steel rotating cylinder anode, *Desalination and Water Treatment*, 300, 2023, 158–166, https://doi.org/10.5004/dwt.2023.29713

[5] T.J. Al-Musawi, G. McKay, P. Rajiv, N. Mengelizadeh, D. Balarak, Efficient sonophotocatalytic degradation of acid blue 113 dye using a hybrid nanocomposite of CoFe2O4 nanoparticles loaded on multi-walled carbon nanotubes, *Journal of Photochemistry and Photobiology A: Chemistry*, 424, 2022, 113617, https://doi.org/10.1016/j.jphotochem.2021.113617

[6] T.J. Al-Musawi, P. Rajiv, N. Mengelizadeh, I.A. Mohammed, D. Balarak, Development of sonophotocatalytic process for degradation of acid orange 7 dye by using titanium dioxide nanoparticles/graphene oxide nanocomposite as a catalyst, *Journal of Environmental Management*, 292, 2021, 112777, https://doi.org/10.1016/j.jenvman.2021.112777

[7] A.B. Salman, R.T. Al-khateeb, S.N. Abdulqahar, Electrochemical removal of crystal violet dye from simulated wastewater by stainless steel rotating cylinder anode: COD reduction and decolorization, *Desalination and Water Treatment*, 320, 2024, 100787, https://doi.org/10.1016/j.dwt.2024.100787

[8] H. Ben Slama, A. Chenari Bouket, Z. Pourhassan, F.N. Alenezi, A. Silini, H. Cherif-Silini, T. Oszako, L. Luptakova, P. Golińska, L. Belbahri, Diversity of Synthetic Dyes from Textile Industries, Discharge Impacts and Treatment Methods, *Applied Sciences*, 11, 2021, 6255, https://doi.org/10.3390/app11146255

[9] Z.H. Jabbar, A.A. Okab, B.H. Graimed, M.A. Issa, S.H. Ammar, Photocatalytic destruction of Congo red dye in wastewater using a novel Ag2WO4/Bi2S3 nanocomposite decorated g-C3N4 nanosheet as ternary S-scheme heterojunction: Improving the charge transfer efficiency, *Diamond and Related Materials*, 133, 2023, 109711, https://doi.org/10.1016/j.diamond.2023.109711

[10] A.G. Saleem, S.M. Al-Jubouri, Efficient Separation of Organic Dyes using Polyvinylidene Fluoride/Polyethylene Glycol-Tin Oxide (PVDF/PEG-SnO2) Nanoparticles Ultrafiltration Membrane, *Applied Science and Engineering Progress*, 2024, https://doi.org/10.14416/j.asep.2024.08.001

[11] A.M. Elgarahy, K.Z. Elwakeel, S.H. Mohammad, G.A. Elshoubaky, A critical review of biosorption of dyes, heavy metals and metalloids from wastewater as an efficient and green process, *Cleaner Engineering and Technology*, 4, 2021, 100209, https://doi.org/10.1016/j.clet.2021.100209

[12] N. Nasseh, T.J. Al-Musawi, R. Khosravi, A.H. Panahi, F.S. Arghavan, B. Barikbin, FeNi3@SiO2@CuS magnetic nanocomposite: synthesizing, characterization, and application for methylene blue adsorption, *Desalination and Water Treatment*, 210, 2021, 402–414, https://doi.org/10.5004/dwt.2021.26456

[13] P.O. Oladoye, T.O. Ajiboye, E.O. Omotola, O.J. Oyewola, Methylene blue dye: Toxicity and potential elimination technology from wastewater, *Results in Engineering*, 16, 2022, https://doi.org/10.1016/j.rineng.2022.100678

[14] B. Zargar, H. Parham, M. Rezazade, Fast Removal and Recovery of Methylene Blue by Activated Carbon Modified with Magnetic Iron Oxide Nanoparticles, *Journal of the Chinese Chemical Society*, 58, 2011, 694–699, https://doi.org/10.1002/jccs.201190108

[15] R. Ahmad, R. Kumar, Adsorption studies of hazardous malachite green onto treated ginger waste, *Journal of Environmental Management*, 91,2010, 1032–1038, https://doi.org/10.1016/j.jenvman.2009.12.016

[16] J. Zhang, Md.S. Azam, C. Shi, J. Huang, B. Yan, Q. Liu, H. Zeng, Poly(acrylic acid) functionalized magnetic graphene oxide nanocomposite for removal of methylene blue, *RSC Advances*, 5, 2015, 32272–32282, https://doi.org/10.1039/C5RA01815C

[17] A.B. Salman, S.N. Abdulqahar, Electrochemical oxidation of methyl blue dye by stainless steel tubes bundle anode, *Desalination and Water Treatment*, 317, 2024, 100133, https://doi.org/10.1016/j.dwt.2024.100133

[18] A.B. Salman, Electrochemical oxidation of methyl orange dye by stainless steel rotating cylinder anode, *International Journal of Environment and Waste Management*, 28, 2021, 114, https://doi.org/10.1504/IJEWM.2021.117012

[19] M.N. Arifin, R. Jusoh, H. Abdullah, N. Ainirazali, H.D. Setiabudi, Recent advances in advanced oxidation processes (AOPs) for the treatment of nitro- and alkyl-phenolic compounds, *Environmental Research*, 229, 2023, 115936, https://doi.org/10.1016/j.envres.2023.115936

[20] Abdullah, S. M., experimental study for oxidation of phenol by fentons reagent, *Journal of Engineering*, 16, 2010, 4547–4556, https://doi.org/10.31026/j.eng.2010.01.12

[21] S.M. Al-Jubouri, H.A. Sabbar, E.M. Khudhair, S.H. Ammar, S. Al Batty, S. Yas Khudhair, A.S. Mahdi, Silver oxide-zeolite for removal of an emerging contaminant by simultaneous adsorption-photocatalytic degradation under simulated sunlight irradiation, *Journal of Photochemistry and Photobiology A: Chemistry*, 442, 2023, 114763, https://doi.org/10.1016/j.jphotochem.2023.114763

[22] A.G. Saleem, S.M. Al-Jubouri, Separation performance of cationic and anionic dyes from water using polyvinylidene fluoride-based ultrafiltration membrane incorporating polyethylene glycol, *Desalination and Water Treatment*, 319, 2024, https://doi.org/10.1016/j.dwt.2024.100546

[23] S.A. Sadek, S.M. Al-Jubouri, S. Al-Batty, Investigating the Fouling Models of the Microfiltration Mixed Matrix Membranes-Based Oxide Nanoparticles Applied for Oil-in-Water Emulsion Separation, *Iraqi Journal of Chemical and Petroleum Engineering*, 25, 2024, 1–16, https://doi.org/10.31699/IJCPE.2024.2.1

[24] V. Vaiano, O. Sacco, D. Pisano, D. Sannino, P. Ciambelli, From the design to the development of a continuous fixed bed photoreactor for photocatalytic degradation of organic pollutants in wastewater, *Chemical Engineering Science*, 137, 2015, 152–160, https://doi.org/10.1016/j.ces.2015.06.023

[25] V. Chakachaka, C. Tshangana, O. Mahlangu, B. Mamba, A. Muleja, Interdependence of Kinetics and Fluid Dynamics in the Design of Photocatalytic Membrane Reactors, *Membranes*, 12, 2022, 745, https://doi.org/10.3390/membranes12080745

[26] T.V.T. VAN, Chemical reactor design optimization and scaleup, (2008).

[27] A.A. Assadi, J. Palau, A. Bouzaza, D. Wolbert, A.A. Assadi, J. Palau, A. Bouzaza, D. Wolbert, Modeling of a continuous photocatalytic reactor for isovaleraldehyde oxidation: Effect of different operating parameters and chemical degradation pathway, *Chemical Engineering Research and Design*, 91, 2013, 1307–1316, https://doi.org/10.1016/J.CHERD.2013.02.020

[28] R.K. Sinnott, Chemical Engineering Design: Chemical Engineering Design v.6: Chemical Engineering Design Vol 6, Chemical Engineering Design, 6, 2005, 1056.

[29] M. S.v., B.K. Tripathy, M. Kumar, S. Pramod, Simultaneous degradation of anionic and cationic dyes from multi-dye systems using falling film photoreactor: performance evaluation, kinetic and toxicity analysis, *Journal of Environmental Chemical Engineering*, 8, 2020, 104486, https://doi.org/10.1016/J.JECE.2020.104486

[30] F. Dalanta, T.D. Kusworo, Synergistic adsorption and photocatalytic properties of AC/TiO2/CeO2 composite for phenol and ammonia–nitrogen compound degradations from petroleum refinery wastewater, *Chemical Engineering Journal*, 434, 2022, https://doi.org/10.1016/J.CEJ.2022.134687

[31] T.D. Kusworo, A.C. Kumoro, N. Aryanti, T.A. Kurniawan, F. Dalanta, N.H. Alias, Photocatalytic polysulfone membrane incorporated by ZnO-MnO2@SiO2 composite under UV light irradiation for the reliable treatment of natural rubber-laden wastewater, *Chemical Engineering Journal*, 451, 2023, 138593, https://doi.org/10.1016/J.CEJ.2022.138593

[32] T.D. Kusworo, A.C. Kumoro, N. Aryanti, H. Hasbullah, D.R.S. Chaesarifa, M.D. Fauzan, F. Dalanta, Developing a robust photocatalytic and antifouling performance of PVDF membrane using spinel NiFe2O4/GO photocatalyst for efficient industrial dye wastewater treatment, *Journal of Environmental Chemical Engineering*, 11, 2023, 109449, https://doi.org/10.1016/j.jece.2023.109449

[33] I. Fatimah, N.I. Prakoso, I. Sahroni, M.M. Musawwa, Y.L. Sim, F. Kooli, O. Muraza, Physicochemical characteristics and photocatalytic performance of TiO2/SiO2 catalyst synthesized using biogenic silica from bamboo leaves, *Heliyon*, 5, 2019, https://doi.org/10.1016/j.heliyon.2019.e02766

[34] A.S. Adday, S.M. Al-Jubouri, Photocatalytic oxidative removal of the organic pollutant from wastewater using recyclable Ag2O@CRA heterojunction photocatalyst, *Case Studies in Chemical and Environmental Engineering*, 10, 2024, 100852, https://doi.org/10.1016/J.CSCEE.2024.100852

[35] A.S. Adday, S.M. Al-Jubouri, Developing a versatile visible-light-driven polyvinylidene fluoride/Ag2O@CRA photocatalytic membrane for efficient treatment of organic pollutants-contained wastewater, *Journal of Water Process Engineering*, 73, 2025, 107713, https://doi.org/10.1016/j.jwpe.2025.107713

[36] E. Erusappan, S. Thiripuranthagan, R. Radhakrishnan, M. Durai, S. Kumaravel, T. Vembuli, N.J. Kaleekkal, Fabrication of mesoporous TiO2/PVDF photocatalytic membranes for efficient photocatalytic degradation of synthetic dyes, *Journal of Environmental Chemical Engineering*, 9, 2021, 105776, https://doi.org/10.1016/J.JECE.2021.105776

[37] H. Luo, M. Yan, Y. Wu, X. Lin, Y. Yan, Facile synthesis of PVDF photocatalytic membrane based on NCQDs/BiOBr/TiO2 heterojunction for effective removal of tetracycline, *Materials Science and Engineering: B*, 265, 2021, https://doi.org/10.1016/j.mseb.2020.114996

[38] T.D. Kusworo, A.C. Kumoro, M. Yulfarida, A new visible-light driven photocatalytic PVDF-MoS2@WO3 membrane for clean water recovery from natural rubber wastewater, *Journal of Water Process Engineering*, 52, 2023, 103522, https://doi.org/10.1016/j.jwpe.2023.103522

[39] D.P. Utomo, T.D. Kusworo, A.C. Kumoro, M.H.D. Othman, Developing a versatile and resilient PVDF/CeO2@GO-COOH photocatalytic membrane for efficient treatment of antibiotic-contaminated wastewater, *Journal of Water Process Engineering*, 56, 2023, https://doi.org/10.1016/j.jwpe.2023.104353

[40] E.B. Lied, C.F.M. Morejon, R.L. de O. Basso, A.P. Trevisan, P.R.S. Bittencourt, F.L. Fronza, Photocatalytic degradation of H2S in the gas-phase using a continuous flow reactor coated with TiO2-based acrylic paint, *Environmental Technology*, 40, 2019, 2276–2289, https://doi.org/10.1080/09593330.2018.1440010

[41] N. Ćelić, N. Banić, I. Jagodić, R. Yatskiv, J. Vaniš, G. Štrbac, S. Lukić-Petrović, Eco-Friendly Photoactive Foils Based on ZnO/SnO2-PMMA Nanocomposites with High Reuse Potential, *ACS Applied Polymer Materials*, 5, 2023, 3792–3800, https://doi.org/10.1021/acsapm.3c00396

[42] A. Azarniya, M. Soltaninejad, M. Zekavat, F. Bakhshandeh, H.R. Madaah Hosseini, C. Amutha, S. Ramakrishna, Application of nanostructured aluminium titanate (Al2TiO5) photocatalyst for removal of organic pollutants from water: Influencing factors and kinetic study, *Materials Chemistry and Physics*, 256, 2020, https://doi.org/10.1016/j.matchemphys.2020.123740

التحلل المحفز بالضوء لصبغة الميثيلين الزرقاء بأستخدام أغشية فلوريد البولي فينيلدين النشطة والمدعّمة بالعامل المساعد Ag_2O@CRA المحفز بالضوء المرئي: تحليل الحركية وتقييم للتكلفة

عبدالمنعم سحاب عداي [١]، سما محمد الجبوري [١،*]، سرحان البطي [٢]

١ قسم الهندسة الكيمياوية، كلية الهندسة، جامعة بغداد، بغداد، العراق

٢ قسم تكنولوجيا الهندسة الكيميائية والعمليات، كلية الجبيل الصناعية، مدينة جبيل الصناعية، المملكة العربية السعودية

الخلاصة

تمت دراسة الحركية الخاصة بعملية التحلل المحفز بالضوء المرئي لصبغة الميثيلين الزرقاء (MB) باستخدام العامل المساعد المتراكب Ag_2O@CRA وأغشية فلوريد البولي فينيلدين (PVDF) النشطة والمدمجة بالعامل المساعد المتراكب (Ag_2O@CRA) بصيغتها PVDF/Ag_2O@CRA. وقد تضمنت الدراسة مقارنة نتائج النماذج الحركية المستندة على البيانات التجريبية لعملية الأكسدة المحفزة بالضوء المرئي لصبغة MB، حيث تم تطبيق ثلاثة نماذج حركية هي: الموديل الصفري، والموديل من الدرجة الأولى الزائف، ونموذج فريندلخ المعدل. أظهرت النتائج أن التحلل المحفز بالضوء المرئي لصبغة MB بأستخدام العامل المساعد Ag_2O@CRA أتبع موديل الحركية من الدرجة الأولى الزائف، بقيمة ثابت معدل سرعة التفاعل الظاهري (k_1) بلغت ٠,١٢٣١ دقيقة$^{-1}$. غشاء فلوريد البولي فينيلدين المطور بنسبة ٠,٣٪ وزناً من Ag_2O@CRA أتبع موديل الحركية من الدرجة الأولى الزائف، وبقيمة ثابت معدل سرعة التفاعل الظاهري بلغت ٠,٠١٩٦ دقيقة$^{-1}$. كذلك، تم استخدام نموذج لانكماير–هنشلوود لوصف الحركية عند استخدام العامل المساعد Ag_2O@CRA بتراكيز أبتدائية من ١٠ إلى ٤٠ ملغم/لتر، وللغشاء PVDF/Ag_2O@CRA بتراكيز أبتدائية من ٥ إلى ٢٠ ملغم/لتر. وقد أظهرت النتائج أن ثابت معدل معدل سرعة التفاعل الفعلي (k_r) بلغ ٠,٨٢٨٦ ملغم/لتر·دقيقة للعامل المساعد Ag_2O@CRA و٠,٢٠٩ ملغم/لتر·دقيقة لغشاء PVDF/Ag_2O@CRA، بينما بلغ ثابت الاتزان للامتزاز (K_{ad}) ٠,٣٢٤٥ لتر/ملغم و٠,٢١٨ لتر/ملغم لكل من العامل المساعد والغشاء على التوالي. كما تم تقدير التكلفة التصنيعية للعامل المساعد Ag_2O@CRA بحوالي ٢,٤٥ دولار أمريكي لكل ١٠ غرام، وللغشاء PVDF/Ag_2O@CRA بحوالي ٧٨ دولاراً أمريكياً لكل متر مربع.

الكلمات الدالة: الحركية، الأكسدة، العامل المساعد المتراكب، الغشاء المحفز بالضوء، فلوريد البولي فينيلدين، الميثيلين الزرقاء.